2-D Terahertz Metallic Photonic Crystals in Parallel-Plate Waveguides

Yuguang Zhao, *Member, IEEE*, and Daniel R. Grischkowsky, *Fellow, IEEE*

***Abstract*—2-D metallic photonic crystals without defects, with point defects, and with a Fabry–Perot (F–P) defect are characterized by terahertz time-domain spectroscopy. The metal parallel-plate waveguide (PPWG) with single TEM-mode propagation is used as a tool to simulate 2-D photonic crystals in free space. The 2-D metallic photonic-crystal structures were fabricated by coating Au on an SU-8 polymer cylinder array. Wide terahertz bandgaps were observed in the photonic crystals within the PPWG. The experimental measurements have excellent agreement to 2-D photonic-crystal theory without defects. Defect modes are observed in the samples with defects and show the F–P defect has a strong localization effect.**

***Index Terms*—Photonic crystals, submillimeter-wave spectroscopy, terahertz, waveguides.**

I. Introduction

STARTING WITH the pioneering work of Yablonovitch [1] and John [2], photonic crystals in both the microwave and terahertz range have been studied experimentally [3]–[40] for over a decade. It has become especially important to connect the recent terahertz work to the extensive microwave literature because all of the terahertz guided wave demonstrations have their microwave counterparts and because, for both terahertz and microwaves, the real part of metal conductivity can be considered to be frequency independent and to be equal to the handbook dc value, in contrast to metallic conductivity at optical frequencies. Compared to microwaves, terahertz phenomena occur at a smaller spatial scale proportional to the shorter wavelengths. The corresponding frequency-dependent losses are higher and the skin depths are smaller, but the basic phenomena are the same. The smaller terahertz spatial scale is especially convenient for the use of quasi-optics and associated techniques. Microwave engineers are well trained to handle terahertz propagation and interconnect design issues on the smaller single chip scale. The growing interest in terahertz applications presents a unique opportunity for the microwave community.

In contrast to the optical frequency range [41], [42], where submicrometer technology is needed to fabricate photonic structures, the microwave range allows for precise hand assembly of photonic crystals composed of identical millimeter- to centimeter-sized components on repetitive lattice spacings with similar dimensions [3]–[40]. Most microwave photonic crystals have consisted of arrays of dielectric or metal spheres, arrays of cylinders, or arrays of square rods, sometimes supported by dielectric templates. These techniques have enabled the construction and experimental characterization of both 2-D [5]–[10], [17], [20], [23]–[26], [28], [29], [31] and 3-D [11], [12], [14]–[16], [18], [19], [22], [27], [30], [37] photonic crystals. Typical photonic crystals are of the order of ten lattice spacings long by 20 spacings wide with lattice spacings of the order of the wavelength. Although point source excitation and detection of the transmitted microwaves through a 3-D photonic crystal was initially used with excellent results [4], the crystals were more commonly characterized by input microwave beams with diameters smaller than the input face of the photonic crystal and radii of curvatures of several times the beam diameters.

An early 3-D terahertz photonic crystal utilized the orderly stacking of dielectric rods and showed a 30-dB photonic bandgap from 0.37 to 0.52 THz [13]. A subsequent 2-D metallic photonic crystal, consisting of a 2-D honeycomb of metal 80-μm-diameter cylinders threaded through two supporting meshes separated by 3 cm, showed strong 10-dB frequency dependence from 0.8 to 1.7 THz [23]. Ten-period-long metal 2-D photonic crystals, constructed with nickel-coated 50-μm-diameter silica cylinders arrayed between parallel 70-μm-square meshes, showed a 90-dB photonic bandgap at 2.2 THz [32]. Deep reactive ion etching has been used to etch 80-μm-square holes on a 100-μm-square lattice through a 500-μm-thick high-resistivity Si wafer [34], which showed a 13-dB photonic bandgap from 0.9 to 1.2 THz [34]. Terahertz time-domain spectroscopy (THz-TDS) transmission studies from 0.2 to 0.4 THz of a hexagonal array of 360-μm-diameter air holes with a 400-μm lattice constant in a 300-μm-thick high-resistivity Si slab within a parallel-plate metal waveguide showed photonic-bandgap features together with an observable defect mode [36]. An air-spaced modular parallel-plate structure with one plate having periodic grooves was developed for biosensing from 0.3 to 0.6 THz [43], and showed sharp transmission features and a $Q = 250$ value defect resonance. More recently, asynchronous optical sampling for such sensors was demonstrated [44].

With respect to our goal of eliminating the above-described arrays of long cylinders to achieve 2-D photonic crystals, we have experimentally demonstrated that the parallel-plate waveguide (PPWG) can be generalized to enable effectively 2-D terahertz embodiments within the bounded space formed by the narrow separation between the two metal plates [45]–[48].

Manuscript received May 18, 2006; revised December 20, 2006. This work was supported in part by the National Science Foundation.

The authors are with the School of Electrical and Computer Engineering, Oklahoma State University, Stillwater, OK 74078 USA (e-mail: grischd@ceat.okstate.edu).

Color versions of one or more of the figures in this paper are available online at http://ieeexplore.ieee.org.

Digital Object Identifier 10.1109/TMTT.2007.892798

The usual formulation of the electromagnetic wave equation in rectangular coordinates, as applied to the PPWG with the plate separation along the y-axis, shows that TEM mode propagation is preserved with included 2-D-shaped (x, z) components [45]–[48]. Within this bounded space, 2-D reflective [47], refractive, and diffractive [48] quasi-optical components have been experimentally demonstrated. The resulting TEM wave propagation is analytically described as 2-D waves (with no y dependence) propagating in the x–z-plane; 2-D circular waves are analogous to 3-D spherical waves, and 2-D line waves are analogous to 3-D plane waves. This situation allows for the effective experimental realization of 2-D situations that can only be approximated in free space.

Here, we report on the adaptation of the above-described cylindrical photonic-crystal microwave structures to 2-D photonic-crystal terahertz structures within the bounded space of the PPWG. These terahertz metallic 2-D photonic crystals were realized by using semiconductor lithographic technology. For our experiments, the previously handcrafted macroscopic photonic-crystal microwave cylindrical structures were transformed into microscopic 2-D photonic-crystal terahertz structures using cleanroom-based lithography to reduce the spatial dimensions by as much as 1/100, corresponding to the increased terahertz frequency. The consequent 70-μm-diameter 80-μm-high metal-coated dielectric cylinders standing on a 160-μm periodic square lattice were ideal for microscopically precise lithographic processing, as shown in Fig. 1.

Our observations of the strongly varying frequency-dependent terahertz transmission through the resulting metallic 2-D photonic-crystal structures were fit with excellent agreement by the transfer matrix method (TMM) theory [49]–[51] for 3-D infinite cylindrical geometry photonic-crystal structures, scaled down in size for terahertz frequencies. The software used for the TMM calculation can only treat nondefect metallic structures [51]. Due to the 2-D embodiment within the bounded space, no correction was needed due to the finite thickness. The excellent agreement also confirms the fabrication quality of the 2-D photonic crystals.

One set of applications of the work presented here would be based on the ability to engineer parallel-plate components with desired transmission properties. These components could be used as narrowband filters with selective transmission or rejection properties. An important application of such high-Q filtering is for biological [43] and chemical sensing. In addition, 2-D photonic-crystal structures within the confines of the PPWG could possibly be used as a high-performance interconnect layer based on 2-D TEM propagation [45]–[48] or a 2-D guided-wave network.

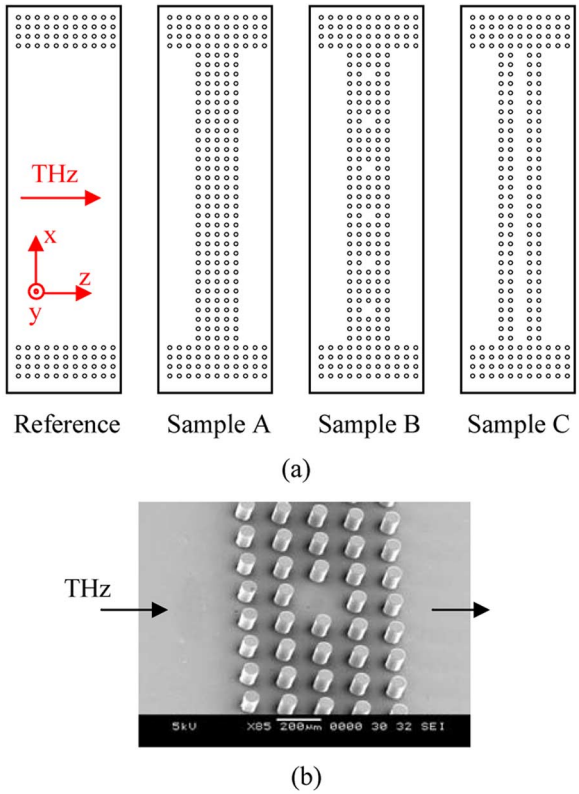

Fig. 1. (a) Not-to-scale schematic diagram of the samples. (b) SEM image of Sample B, where the total length across the 5-C array is $4 \times 160\ \mu\text{m} + 70\ \mu\text{m} = 0.71$ mm. The sample chip size is 25-mm wide $\times$ 10-mm long (terahertz path) $\times$ 0.4-mm thick. The centered 5-C arrays of the samples extend the full 25-mm width of the sample chip and are 0.71-mm long. The 2.5-mm-wide $\times$ 10-mm-long spacer arrays, best shown on the reference chip, have the same pattern and 80-μm height as the sample arrays.

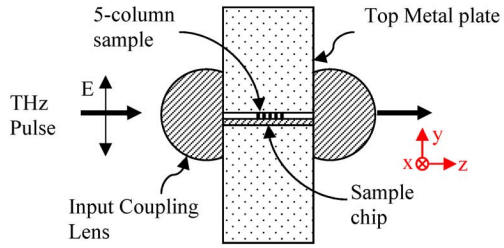

Fig. 2. Cross-sectional view of the PPWG assembly. The centered 5-C's of the 10-mm-long sample chip are shown together with the two silicon lenses used to couple the terahertz pulse into and out of the PPWG formed by the top metal plate and the top metallized surface (Au on Al) of the sample or reference chip, separated by the 80-μm height of the cylinders. There is no terahertz propagation through the Si substrate of the sample or reference chip. The length of the entire structure along the terahertz beam direction is [6.56 mm (input lens) + 10.00 mm (sample chip) + 6.56 mm (output lens)] = 23.12 mm long. The height of assembly is [8 mm (top metal plate) + 80 μm (column height) + 0.4 mm (sample chip thickness) + 8 mm (bottom metal plate)] = 16.48 mm. The lenses extend 15.0 mm perpendicular to the plane of the figure and the metal plates and the sample plates extend 25.0 mm.

II. Fabrication and Experiment

For fabricating high-quality terahertz 2-D metallic photonic-crystal structures, microelectromechanical systems (MEMS) [52] and metallization technologies were employed [36], [38]. First, SU-8 2025 negative photoresist from MicroChem Inc., Newton, MA, was spun onto a 3-in Al coated silicon wafer to form an 80-μm-thick film. With a custom designed lithographic mask, the SU-8 film was exposed and developed. After the lithography, the soft SU-8 structures on the wafer were baked at 150 °C, which transformed them into permanent hard polymer structures. The 0.4-mm-thick wafer was diced into 25-mm-wide $\times$ 10.00-mm-long chips to fit the PPWG setup, as shown in Fig. 2. The 400-nm-thick Au film metallization of the chips was then conducted in an Au sputter coater. The good step coverage property of sputtering provided the required Au film quality on the sidewall of the cylinders.

The metallic photonic crystals consist of a square array of m rows and n columns of cylinders in air with lattice constant $L = 160$ μm, diameter $d = 70$ μm, and height $h = 80$ μm. The number m of rows in the columns was $126 = (20\,\text{mm}/160\,\mu\text{m})+1$. Three different samples with five-column (5-C) arrays of cylinders were fabricated. As shown in Fig. 1(a), Sample A has 5-C cylinders without any defects, Sample B has 5-C cylinders with the removal of one cylinder every five rows from the center column, and Sample C has 5-C cylinders with the removal of the center column to form the Fabry–Perot (F–P) defect cavity. Fig. 1(b) shows a scanning electron microscope (SEM) image of Sample B. The structures on the two sides of the chips were used as the spacers, which have the same height as the cylinders in the center. The reference chip has the same spacer structures, but no cylinders in the center [see Fig. 1(a)].

The 2-D terahertz photonic crystals were completed by sandwiching a sample chip between the two polished Al plates of the original PPWG. The 80-μm spacers separated the top Al plate and the regions of unstructured metal surface of the sample or reference chip. As shown in Figs. 1 and 2, the terahertz pulse propagation was perpendicular to the columns of cylinders, with the polarization parallel to the cylinders. The resulting 2-D photonic crystals, centered within the 10.00-mm-long waveguide assembly, were characterized by the THz-TDS system [53].

To initiate the THz-TDS characterization, the terahertz reference pulse transmitted through the waveguide assembly with the reference chip installed was measured. The terahertz reference pulse propagated in the TEM mode through the 10.00-mm-long 80-μm air-spaced PPWG formed by the top metal plate and the metallized unstructured surface of the reference chip. The reference chip was then replaced by the sample chip and the transmitted terahertz sample pulse was measured. For THz-TDS, the terahertz sample pulses are quantitatively compared to the terahertz reference pulse. From the comparison of the corresponding complex amplitude spectra, the linear transfer function $H(\omega)$ describing the complex filtering effect of the sample is obtained. In the measurement, the in-coupled terahertz pulse first propagates through 4.65 mm of the unstructured PPWG before entering the 5-C pattern of the sample chip. After traversing the 0.71-mm path length of the 5-C sample pattern, the terahertz pulse traverses another 4.65-mm length of the unstructured PPWG before out-coupling to the receiver. The terahertz receiver is polarization sensitive with an amplitude rejection ratio of approximately 5 : 1.

Two plano-cylindrical high-resistivity uncoated silicon lenses (Fig. 2) were used to couple the terahertz pulse into and out of the PPWG structures of reference or samples. The lenses are 15 mm $\times$ 10 mm $\times$ 6.56 mm with a 5-mm radius of curvature. The input Si lens focuses the incoming terahertz pulse to an elliptical spot with the minor axis of 150 μm, perpendicular to the waveguide plates, and the linearly wavelength-dependent major axis of 9 mm at 1 THz, parallel to the waveguide plates, compared to the 20-mm clear width of the sample chips.

The quasi-optical coupling of a freely propagating terahertz beam into the PPWG at the beam waist of a confocal terahertz system is surprisingly efficient over the entire bandwidth. Compared to the free-space system, the insertion of only the two cylindrical lenses separated by their focal lengths reduces the amplitude of the transmitted terahertz pulse by the multiplicative factor $0.4 = 0.8 \times 0.5$, where 0.5 is the Fresnel transmission through the uncoated Si lenses (due to the reflective losses of four surfaces), and 0.8 is the quasi-optical amplitude coupling (transmission) through the two confocal lenses. In the initial demonstration [45], when the foci of the two lenses were separated by a 12.6-mm-long 108-μm air-spaced Cu PPWG, the amplitude transmission was reduced to $0.32 = 0.8 \times 0.8 \times 0.5$, similar to the situation for the experiment described here. The additional factor of 0.8 is mainly due to the waveguide coupling loss with a smaller loss due to waveguide absorption. In comparison to the received terahertz power of the free-space system, the waveguide assembly of Fig. 2 with the reference plate installed reduces the received power by 10 dB, where 6 dB is due to the Fresnel reflection losses from the lenses and the remaining 4 dB is the quasi-optical coupling loss. Clearly, reducing the reflective losses would be helpful. As suggested by one of the referees of this paper, a thin parylene antireflection coating on the lenses could prove effective to reduce these losses [54].

At the confocal beam waist of the employed THz-TDS system, there are 30 wavelengths across the 9-mm-diameter beam at 1 THz, similar to the 30–50 in the microwave experiments [9]. The frequency-independent 2-D THz beam divergence is 0.033 rad, which is also the angular acceptance of the terahertz receiver. This narrow acceptance angle of the terahertz receiver is important for accurate measurements because the forward (zeroth order) transmission through the photonic crystals is expected to be sharply angular dependent, similar to a transmission grating, requiring good angular resolution to obtain the proper on-axis signal strength.

III. Results and Discussion

Fig. 3 shows the transmitted TEM-mode terahertz pulse with the reference chip installed in the waveguide assembly and the corresponding amplitude spectrum, which are similar to the terahertz pulse and spectrum in free space. The reference pulse is only shown to 10 ps to detail the pulse shape; the complete scan extended to 30 ps. As discussed above, the incoming terahertz beam, focused by the cylindrical Si lens, has been shown to couple with exceptional efficiency to the TEM (TM_0) mode of the PPWG [45]–[48].

This TM_0-mode selectivity is due to the following properties. For the linear terahertz polarization perpendicular to the waveguide plates, coupling is possible only to the TM modes. For the 80-μm plate separation, the cutoff frequencies of the $\mathrm{TM}_1, \mathrm{TM}_2$, and TM_3 modes are 1.88, 3.75, and 5.62 THz, respectively. By symmetry arguments, the overlap integral of the focused incoming terahertz beam with the TM_1 mode at the waveguide face is zero, thereby giving no coupling. Furthermore, the terahertz beam at focus is broad enough so that the overlap integral is very small for the TM_2 mode, and coupling is negligible. Finally, our spectral range is below cutoff for the TM_3 mode. For completeness and comparison, we note the comprehensive work on micromachined rectangular waveguides for millimeter-wave and terahertz frequencies [55], [56].

Fig. 4(a) and (b) shows the transmitted terahertz pulse with the Sample A chip and the corresponding amplitude spectrum. The transmitted pulse from the sample has a ringing structure

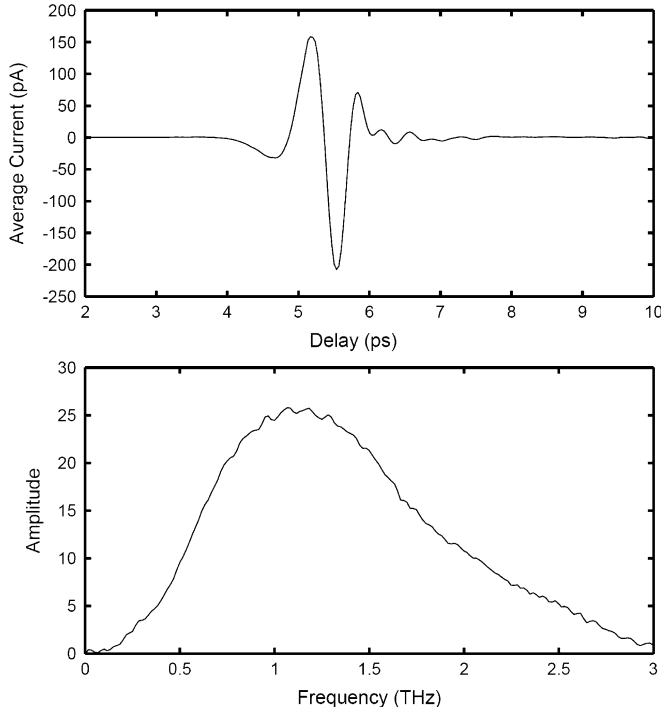

Fig. 3. Transmitted terahertz pulse with the reference chip in place and the corresponding amplitude spectrum. The measured terahertz pulse amplitude expressed in picoamperes [53] is linearly proportional to the electric field amplitude.

extending to 25 ps. There is a small 0.2-ps propagation delay of the sample pulse with respect to the reference pulse. From the spectrum, it is clear that the first two bandgaps extend from low frequency to 1.0 THz and from 1.2 to 1.6 THz.

To enable our theoretical modeling of these results, we will now show that within the approximations of the simple Drude model, the real part of the dielectric constant of metal is a negative constant, while the much larger imaginary part is, to a good first-order approximation, proportional to the wavelength. The simple Drude model [57] treats the free carriers in a metal as classical point charges subject to random collisions for which the collision damping is independent of the carrier velocity. According to the model, the frequency-dependent complex dielectric constant ε (the square of the complex index of refraction $n = n_r + in_i$) is given in SI units as

$$\varepsilon = \varepsilon_\infty + i\sigma/(\varepsilon_0\omega) = \varepsilon_\infty - \omega_p^2/\omega(\omega + i\Gamma) \tag{1}$$

where the corresponding Drude complex conductivity is given by

$$\sigma = \sigma_{\rm dc} i\Gamma/(\omega + i\Gamma) = i\varepsilon_0\omega_p^2/(\omega + i\Gamma). \tag{2}$$

For the above relationships, ε_∞ is the contribution of the bound electrons, and $\Gamma = 1/\tau$ is the damping rate, where τ is the average collision time. The plasma angular frequency ω_p is defined by $\omega_p^2 = Ne^2/(\varepsilon_0 m)$, where N is the number density of carriers, e is the electronic charge, ε_0 is the free-space permittivity, and m is the effective carrier mass. The dc conductivity $\sigma_{\rm dc}$ is given by $\sigma_{\rm dc} = e\,\mu{\rm N}$ with the mobility $\mu = e/(m\Gamma)$.

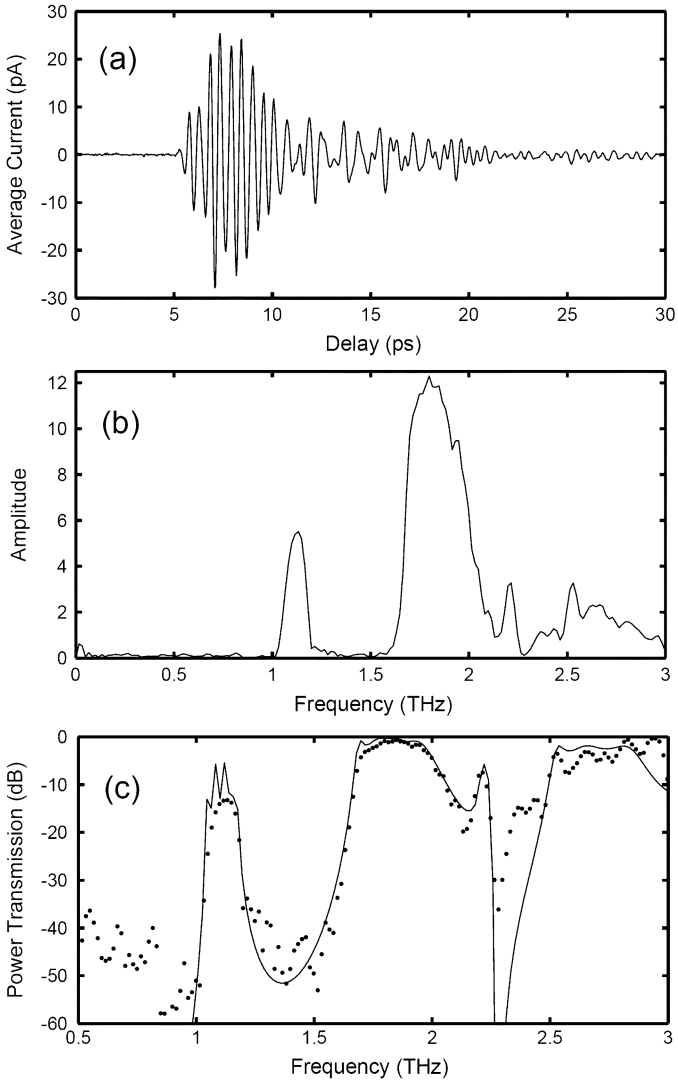

Fig. 4. (a) Transmitted terahertz pulse with the Sample A chip in place. (b) Amplitude spectrum of transmitted terahertz pulse. (c) Power transmission in decibels with Sample A (dots) and numerical simulation (solid line). The power transmission is the square of the ratio of the measured spectral amplitude of (b) to the measured spectral amplitude of the reference pulse of Fig. 3(b), i.e., Fig. 4(b)/Fig. 3(b).

The above expression for ε can be rewritten in the form

$$\varepsilon = \varepsilon_\infty - \frac{\sigma_{\rm dc}\Gamma}{\varepsilon_0\omega(\omega + i\Gamma)} = \varepsilon_\infty + \frac{i\sigma_{\rm dc}}{\varepsilon_0\omega(1 - i\omega/\Gamma)}. \tag{3}$$

For the microwave and terahertz frequency ranges, the ratio $\omega/\Gamma \ll 1$, and the above expression for ε is, to a good first-order approximation, given by

$$\varepsilon \approx \varepsilon_\infty - \sigma_{\rm dc}/(\varepsilon_0\Gamma) + i\sigma_{\rm dc}/(\varepsilon_0\omega). \tag{4}$$

For the case of conducting metals ε can, to an excellent approximation, be further reduced to

$$\varepsilon \approx -\sigma_{\rm dc}/(\varepsilon_0\Gamma) + i\sigma_{\rm dc}/(\varepsilon_0\omega). \tag{5}$$

It is important to note that even though the conductivity is considered to be frequency independent and equal to the dc

value $\sigma_{\rm dc}$, the above argument shows in (5) that the resulting dielectric constant for conducting metals has a negative constant real part and a much larger frequency-dependent imaginary part.

It is possible to consider microwave and terahertz pulse propagation within a conducting metal, by rewriting the dielectric constant ε in the equivalent form involving the complex index of refraction $n = n_r + in_i$ as follows:

$$\varepsilon = n^2 = n_r^2 - n_i^2 + i2n_r n_i. \tag{6}$$

Within the approximation, good for microwave and terahertz frequencies, that $\omega \ll \Gamma$, (5) yields the relationship

$$n_r \approx n_i \approx [\sigma_{\rm dc}/(2\omega\varepsilon_0)]^{1/2} \tag{7}$$

which is consistent with the similar result for metals obtained from optical theory [58]. The standard Fresnel relations in complex form describe the reflection and transmission coefficients for the metal [58]. Propagation within the metal is described by the simple relationship $\exp(ikz - \omega t)$, where $k = 2\pi(n_r + in_i)/\lambda_o$. The skin depth δ is seen in the relationship $\exp(-2\pi n_i z/\lambda_o) = \exp(-z/\delta)$. Using (7), the skin depth is obtained as

$$\delta = c[\varepsilon_0/(\pi f\sigma_{\rm dc})]^{1/2} = 1/[(\pi f\mu_0\sigma_{\rm dc})]^{1/2} \tag{8}$$

which is the usual microwave result [59], [60].

To perform the TMM numerical simulation [49]–[51], we need the plasma frequency ω_p and the damping rate Γ, which are related to $\sigma_{\rm dc}$ by $\sigma_{\rm dc}\Gamma = \varepsilon_0\omega_p^2$. Given the measurement of $\Gamma/2\pi = 6.5$ THz for gold [61], and the handbook Au conductivity of $\sigma_{\rm dc} = 4.10 \times 10^7/(\Omega \cdot {\rm m})$ [60], ω_p is calculated by the relationship $\omega_p = (\sigma_{\rm dc}\Gamma/\varepsilon_0)^{1/2}$ to be $\omega_p/2\pi = 2\,190$ THz.

Fig. 4(c) compares the measured power transmission for Sample A and the simulated power transmission of a 5-C, infinitely long, and wide array of solid Au cylinders similar to Sample A. Beyond 1 THz, the results fit very well. However, below 1 THz, there is significant difference considered to be due to the 40-dB dynamic range capability of the THz-TDS measurement. If we take -30 dB as the threshold, the measured bandgaps are from 0.25 to 1.04 THz and from 1.20 to 1.62 THz. In comparison, the calculated bandgaps are from 0 to 1.03 THz and from 1.19 to 1.60 THz. The corresponding positions of the dips and peaks of the experimental results are in good agreement with the theory.

Fig. 5(a) and (b) shows the transmitted terahertz pulse and the corresponding amplitude spectrum with Sample B. Fig. 5(c) compares the power transmission for Sample B with Sample A. The transmissions are similar, except that for Sample B, the power transmission at 1.1 THz has been reduced by approximately the multiplicative factor 0.2 compared to Sample A. This reduction is considered to be due to scattering by the point defects of Sample B. The defect of Sample B is responsible for the relatively weak peak (defect mode) at 1.42 THz in the second bandgap from 1.2 to 1.6 THz. The peak has 0.2% power transmission. This small value is considered to be caused by the point symmetry of the defect not being compatible with the propagating line wave. Similar metallic photonic structures (solid copper rods, $r/L = 0.2$) have been theoretically studied using

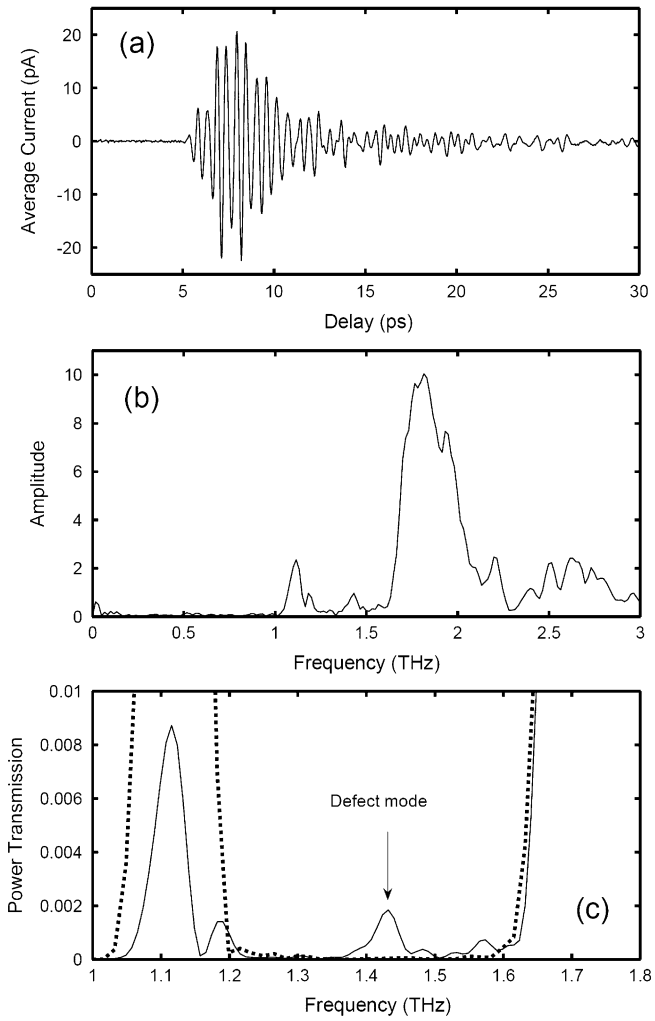

Fig. 5. (a) Transmitted terahertz pulse with the Sample B chip in place. (b) Amplitude spectrum of transmitted pulse. (c) Power transmission with Sample B (solid line) compared to the power transmission with Sample A (dotted line).

the finite-difference time-domain method [62]. In [62], the resonant frequency for one defect mode is given by the numerical result $f_0 = 0.753$ (c/L), where c is the speed of light. For our case, the corresponding theoretical frequency is 1.412 THz, which is in good agreement with our observation of 1.42 THz (gold coated rods, $r/L = 0.22$).

To gain higher transmission of the defect mode, Sample C with the F–P defect was measured. Fig. 6(a) and (b) shows the transmitted terahertz pulse and the corresponding amplitude spectrum for Sample C. Here, the peak pulse amplitude and peak transmitted spectra are clearly larger than for Sample A, demonstrating the transmission enhancement of the F–P defect. Fig. 6(c) shows the comparison of the power transmission for Sample A and Sample C. Compared to the power transmission peak of Sample A centered at 1.13 THz with a full width at half maximum (FWHM) of $\Delta f = 80$ GHz and a peak value of 5%, for Sample C, this peak has shifted to 1.10 THz, narrowed to $\Delta f = 20$ GHz and increased to 18.5%. The Q value of this transmission maximum is evaluated as $f/\Delta f = 1.10$ THz/0.020THz $= 55$. Similar to Sample B, there is a peak

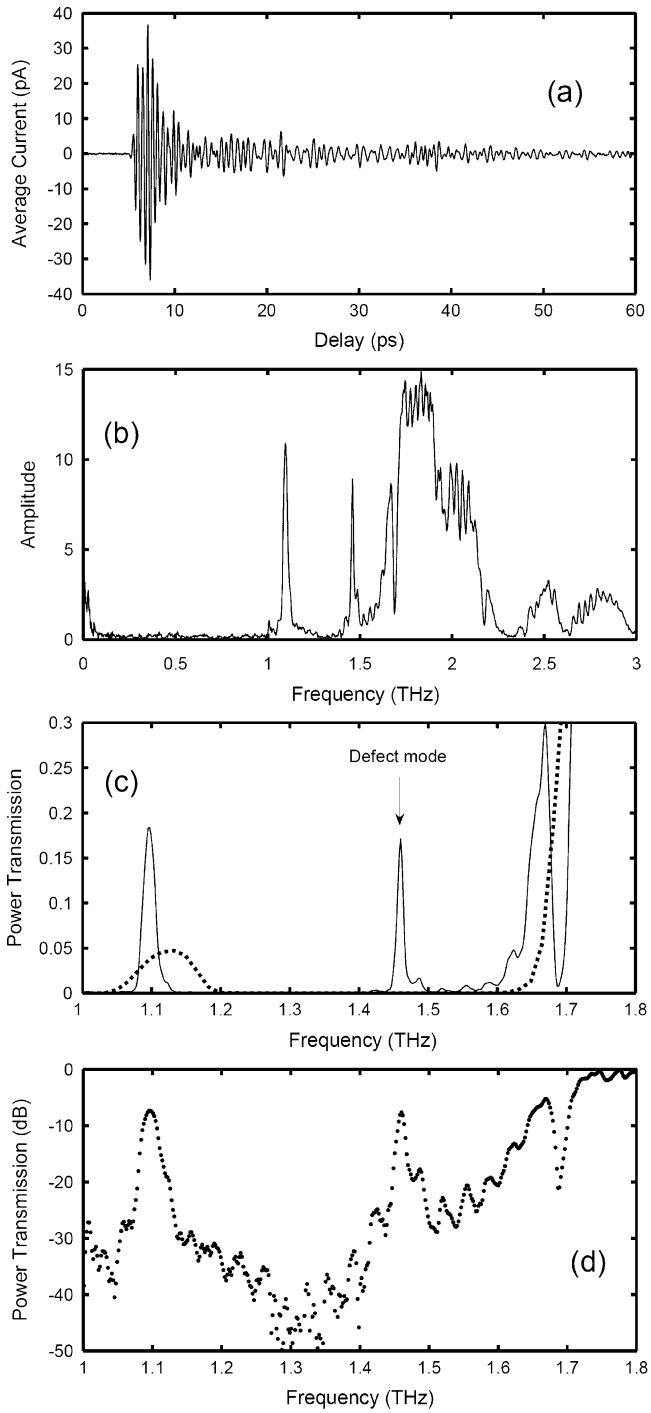

Fig. 6. (a) Transmitted terahertz pulse with the Sample C chip in place. (b) Amplitude spectrum of transmitted pulse. (c) Power transmission with Sample C (solid line) compared to the power transmission of Sample A (dotted line). (d) Power transmission in decibels with Sample C.

(defect mode) in the second bandgap from 1.2 to 1.6 THz of Sample C. The position of this peak at 1.46 THz has shifted approximately 0.04 THz from Sample B because of mode coupling effects [24] and experimental variation. The peak with 17% power transmission shows very strong localization compared with the point defect of Sample B. This peak at 1.46 THz has a FWHM linewidth of $\Delta f = 11$ GHz, corresponding to the relatively high-Q value of 133. The high strength and high Q of this F–P defect is thought to arise from the compatible symmetry with the propagating 2-D line wave. We consider that the $Q = 133$ value may be limited by the small number (only two) of columns on either side of the defect. One can also observe a sharp transmission minimum centered at 1.69 THz with a FWHM linewidth of 30 GHz and with the peak power transmission falling from 33% to 1% on the line center. In order to present the dynamic range of the transmission resonances for Sample C, the observations were replotted in decibels in Fig. 6(d), showing the 24-dB transmission peak at 1.10 THz, the 20-dB F–P defect transmission resonance peak at 1.46 THz, and the 17-dB transmission minimum at 1.69 THz.

The defect mode frequency f_r in the F–P defect can be calculated by the F–P resonance condition $f_r = (2m\pi - \phi)c/(4\pi L)$, where m is the mode number, ϕ is the total phase contribution of two mirrors, and L is the separation between the mirrors [16]. Here, the separation $L = 160$ μm is the width of one column spacing. There is no separation for the full column structure (Sample A). When one column is removed, the separation is equal to the column spacing. For the defect mode at 1.46 THz, m is evaluated as 2 and ϕ as 159°.

For completeness, we compare these results with our unsuccessful first attempt to create and characterize 2-D metallic photonic crystals [38]. Initially, we used a 2-D photonic crystal of sputtered metal coated cylinders, 70-μm tall, 70-μm diameter, and arranged on a 160-μm-square lattice, lithographically fabricated on a 25.4-mm-square Si plate, which filled the space between the plates of the longer PPWG. However, due to the large number of metal coated columns ($n = 160$), there was no observable terahertz transmission through this structure. In order to obtain some transmission, we broke the 2-D symmetry by increasing the space between the waveguide plates to let the tops of the metal coated cylinders form a 100-μm airgap to the second plate. This (theoretically undescribed) photonic waveguide showed strong photonic transmission effects, with stopbands or transmission features having instrument-limited 40-dB contrasts [38].

We then studied the more transparent dielectric 2-D photonic crystals incorporated into the PPWG [40]. The dielectric 2-D crystals consisted of 65-μm-diameter 70-μm-high dielectric cylinders standing on a 160-μm-square lattice and were characterized by THz-TDS from 0.2 to 3 THz. These dielectric 2-D photonic crystals of four-, eight-, and 60-column arrays of cylinders (with no defects) showed high dynamic range, and complex frequency response, including well-formed 40-dB photonic bandgaps in exceptional agreement with 2-D theory [51].

IV. Conclusion

The measurements and characterizations of effective 2-D metallic photonic crystals have been presented in the terahertz range. Wide bandgaps from 0 to 1.0 THz and from 1.2 to 1.6 THz were realized in the metallic photonic crystals, which fit well with the simulation results. Strong localizations of the point defect mode and the F–P defect were also observed. The convenient fabrication method and powerful metal PPWG setup may enable applications, such as terahertz metallic photonic-crystal cavities and photonic networks.

The fact that these 2-D photonic-crystal structures were lithographically fabricated using custom designed lithographic masks demonstrates that any 2-D photonic-crystal geometry consistent with the broad applicability of lithography can be achieved. Furthermore, the fact that the theoretical simulations agree with experiment will allow for accurate simulations of proposed structures before mask design and fabrication. Consequently, this study has shown the possibility of design and fabrication of 2-D photonic crystals within the PPWG with specified frequency-dependent transmission.

ACKNOWLEDGMENT

The authors thank M. Gong, Oklahoma State University, Stillwater, for technical support and A. Bingham, Oklahoma State University, and N. Laman, Oklahoma State University, for helpful discussions.

REFERENCES

[1] E. Yablonovitch, "Inhibited spontaneous emission in solid-state physics and electronics," *Phys. Rev. Lett.*, vol. 58, no. 20, pp. 2059–2062, May 1987.

[2] S. John, "Strong localization of photons in certain disordered dielectric superlattices," *Phys. Rev. Lett.*, vol. 58, no. 23, pp. 2486–2489, Jun. 1987.

[3] E. Yablonovitch, T. J. Gmitter, and K. M. Leung, "Photonic band structure: The face-centered-cubic case employing nonspherical atoms," *Phys. Rev. Lett.*, vol. 67, no. 17, pp. 2295–2298, Oct. 1991.

[4] E. Yablonovitch, T. J. Gmitter, R. D. Meade, A. M. Rappe, K. D. Brommer, and J. D. Joannopoulos, "Donor and acceptor modes in photonic band structure," *Phys. Rev. Lett.*, vol. 67, no. 24, pp. 3380–3383, Dec. 1991.

[5] S. L. McCall, P. M. Platzman, R. Dalichaouch, D. Smith, and S. Schultz, "Microwave propagation in two-dimensional dielectric lattices," *Phys. Rev. Lett.*, vol. 67, no. 15, pp. 2017–2020, Oct. 1991.

[6] W. M. Robertson, G. Arjavalingam, R. D. Meade, K. D. Brommer, A. M. Rappe, and J. D. Joannopoulos, "Measurement of photonic band structure in a two-dimensional periodic dielectric array," *Phys. Rev. Lett.*, vol. 68, no. 13, pp. 2023–2026, Mar. 1992.

[7] D. R. Smith, R. Dalichaouch, N. Kroll, S. Schultz, S. L. McCall, and P. M. Platzman, "Photonic band structure and defects in one and two dimensions," *J. Opt. Soc. Amer. B, Opt. Phys.*, vol. 10, no. 2, pp. 314–321, Feb. 1993.

[8] W. M. Robertson, G. Arjavalingam, R. D. Meade, K. D. Brommer, A. M. Rappe, and J. D. Joannopoulos, "Measurement of the photon dispersion relation in two-dimensional ordered dielectric arrays," *J. Opt. Soc. Amer. B, Opt. Phys.*, vol. 10, no. 2, pp. 322–327, Feb. 1993.

[9] D. R. Smith, S. Schultz, N. Kroll, M. Sigalas, K. M. Ho, and C. M. Soukoulis, "Experimental and theoretical results for a two-dimensional metal photonic bandgap cavity," *Appl. Phys. Lett.*, vol. 65, no. 5, pp. 645–647, Aug. 1994.

[10] S. Y. Lin and G. Arjavalingam, "Photonic bound states in two-dimensional photonic crystals probed by coherent-microwave transient spectroscopy," *Opt. Soc. Amer. B, Opt. Phys.*, vol. 11, pp. 2124–2127, Oct. 1994.

[11] E. Ozbay, E. Michel, G. Tuttle, R. Biswas, M. Sigalas, and K.-M. Ho, "Micromachined millimeter-wave photonic bandgap crystals," *Appl. Phys. Lett.*, vol. 64, no. 16, pp. 2059–2061, Apr. 1994.

[12] E. Ozbay, A. Abeyta, G. Tuttle, M. Tringides, R. Biswas, C. T. Chan, C. M. Soukoulis, and K. M. Ho, "Measurement of a three-dimensional photonic bandgap in a crystal structure made of dielectric rods," *Phys. Rev. B, Condens. Matter*, vol. 50, no. 3, pp. 1945–1949, Jul. 1994.

[13] E. Ozbay, E. Michel, G. Tuttle, R. Biswas, K. M. Ho, J. Bostak, and D. M. Bloom, "Terahertz spectroscopy of three-dimensional photonic bandgap crystals," *Opt. Lett.*, vol. 19, no. 15, pp. 1155–1157, Aug. 1994.

[14] E. R. Brown and O. B. McMahon, "Large electromagnetic stop bands in metallodielectric photonic crystals,," *Appl. Phys. Lett.*, vol. 67, no. 15, pp. 2138–2140, Oct. 1995.

[15] E. Ozbay, G. Tuttle, M. Sigalas, C. M. Soukoulis, and K. M. Ho, "Defect structures in a layer-by-layer photonic bandgap crystal," *Phys. Rev. B, Condens. Matter*, vol. 51, no. 20, pp. 13961–13965, May 1995.

[16] E. Ozbay and B. Temelkuran, "Reflection properties and defect formation in photonic crystals," *Appl. Phys Lett.*, vol. 69, no. 6, pp. 743–745, Aug. 1996.

[17] S.-Y. Lin, V. M. Hietala, S. K. Lyo, and A. Zaslavsky, "Photonic bandgap quantum well and quantum box structures: A high Q resonant cavity," *Appl. Phys. Lett.*, vol. 68, no. 23, pp. 3233–3235, Jun. 1996.

[18] J. S. McCalmont, M. M. Sigalas, G. Tuttle, K.-M. Ho, and C. M. Soukoulis, "A layer-by-layer metallic photonic bandgap structure," *Appl. Phys. Lett.*, vol. 68, no. 19, pp. 2759–2761, May 1996.

[19] E. Ozbay, B. Temelkuran, M. Sigalas, G. Tuttle, C. M. Soukoulis, and K. M. Ho, "Defect structures in metallic photonic crystals," *Appl. Phys. Lett.*, vol. 69, no. 25, pp. 3797–3799, Dec. 1996.

[20] F. Gadot, A. Chelnokov, A. De Lustrac, P. Crozat, J. M. Lourtioz, D. Cassagne, and C. Jouanin, "Experimental demonstration of complete photonic bandgap in graphite structure," *Appl. Phys. Lett.*, vol. 71, no. 13, pp. 1780–1782, Sep. 1997.

[21] M. C. Wanke, O. Lehmann, K. Muller, Q. Wen, and M. Stuke, "Laser rapid prototyping of photonic bandgap microstructures," *Science*, vol. 275, pp. 1284–1286, Feb. 1997.

[22] A. Kao, K. A. McIntosh, O. B. McMahon, R. Atkins, and S. Verghese, "Calculated and measured transmittance of metallodielectric photonic crystals incorporating flat metal elements," *Appl. Phys. Lett.*, vol. 73, no. 2, pp. 145–147, Jul. 1998.

[23] C. Jin, B. Cheng, Z. Li, D. Zhang, L. M. Li, and Z. Q. Zhang, "Two dimensional metallic photonic crystal in the THz range," *Opt. Commun.*, vol. 166, pp. 9–13, Aug. 1999.

[24] F. Gadot, A. de Lustrac, J.-M. T. Brillat, A. Ammouche, and E. Akmansoy, "High-transmission defect modes in two-dimensional metallic photonic crystals," *J. Appl. Phys.*, vol. 85, no. 12, pp. 8499–8501, Jun. 1999.

[25] G. Guida, T. Brillat, A. Ammouche, F. Gadot, A. De Lustrac, and A. Priou, "Dissociating the effect of different disturbances on the bandgap of a two-dimensional photonic crystal," *J. Appl. Phys.*, vol. 88, no. 8, pp. 4491–4497, Oct. 2000.

[26] H. Kitahara, N. Tsumura, H. Kondo, M. W. Takeda, J. W. Haus, Z. Yuan, N. Kawai, K. Sakoda, and K. Inoue, "Terahertz wave dispersion in two-dimensional photonic crystals," *Phys. Rev. B, Condens. Matter*, vol. 64, pp. 045202-1–045202-4, Jun. 2001.

[27] B. Temelkuran, M. Beyindir, E. Ozbay, J. P. Kavanaugh, M. M. Sigalas, and G. Tuttle, "Quasimetallic silicon micromachined photonic crystals," *Appl. Phys. Lett.*, vol. 78, no. 3, pp. 264–266, Jan. 2001.

[28] M. Bayindir, E. Cubukcu, I. Bulu, T. Tut, E. Ozbay, and C. M. Soukoulis, "Photonic band gaps, defect characteristics, and waveguiding in two-dimensional disordered dielectric and metallic photonic crystals," *Phys. Rev. B, Condens. Matter*, vol. 64, pp. 195113-1–195113-7, Oct. 2001.

[29] N. Katsarakis, M. Bender, L. Singleton, G. Kiriakidis, and C. M. Soukoulis, "Two-dimensional metallic photonic bandgap crystals fabricated by LIGA," *Microsyst. Tech.*, vol. 8, no. 2–3, pp. 74–77, May 2002.

[30] A. Serpenguzel, "Transmission characteristics of metallodielectric photonic crystals and resonators," *IEEE Microw. Wireless Compon. Lett.*, vol. 12, no. 4, pp. 134–136, Apr. 2002.

[31] P. Gay-Balmaz, C. Maccio, and O. J. F. Martin, "Microwire arrays with plasmonic response at microwave frequencies," *Appl. Phys. Lett.*, vol. 81, no. 15, pp. 2896–2898, Oct. 2002.

[32] S.-W. Wang, W. Lu, X.-S. Chen, Z.-F. Li, X.-C. Shen, and W. Wen, "Two-dimensional photonic crystal at THz frequencies constructed by metal-coated cylinders," *J. Appl. Phys.*, vol. 93, no. 11, pp. 9401–9403, Jun. 2003.

[33] D. Wu, N. Fang, C. Sun, X. Zhang, W. J. Padilla, D. N. Basov, D. R. Smith, and S. Schultz, "Terahertz plasmonic high pass filter," *Appl. Phys. Lett.*, vol. 83, no. 1, pp. 201–203, Jul. 2003.

[34] N. Jukam and M. S. Sherwin, "Two-dimensional terahertz photonic crystals fabricated by deep reactive ion etching in Si," *Appl. Phys. Lett.*, vol. 83, no. 1, pp. 21–23, Jul. 2003.

[35] T. D. Drysdale, R. J. Blaikie, and D. R. S. Cumming, "Calculated and measured transmittance of a tunable metallic photonic crystal filter for terahertz frequencies," *Appl. Phys. Lett.*, vol. 83, no. 26, pp. 5362–5364, Dec. 2003.

[36] Z. Jian, J. Pearce, and D. Mittleman, "Defect modes in photonic crystal slabs studied using terahertz time-domain spectroscopy," *Opt. Lett.*, vol. 29, no. 17, pp. 2067–2069, Sep. 2004.

[37] M. Golosovsky, Y. Neve-Oz, D. Davidov, and A. Frenkel, "Phase shift on reflection from metallodielectric photonic bandgap materials," *Phys. Rev. B, Condens. Matter*, vol. 70, pp. 115105-1–115105-10, Sep. 2004.

[38] A. Bingham, Y. Zhao, and D. Grischkowsky, "THz parallel plate photonic waveguides," *Appl. Phys. Lett.*, vol. 87, Jul. 2005, 051101.

[39] Z. Jian, J. Pearce, and D. M. Mittleman, "Two-dimensional photonic crystal slabs in parallel-plate metal waveguides studied with terahertz time-domain spectroscopy," *Semiconduct. Sci. Technol.*, vol. 20, pp. S300–S306, Jun. 2005.
[40] Y. Zhao and D. Grischkowsky, "Terahertz demonstrations of effectively two-dimensional photonic bandgap structures," *Opt. Lett.*, vol. 31, no. 10, pp. 1534–1536, May 2006.
[41] J. D. Joannopoulos, P. R. Villeneuve, and S. Fan, "Photonic crystals: Putting a new twist on light," *Nature*, vol. 386, pp. 143–149, Mar. 1997.
[42] I. El-Kady, M. M. Sigalas, R. Biswas, K. M. Ho, and C. M. Soukoulis, "Metallic photonic crystals at optical wavelengths," *Phys. Rev. B, Condens. Matter*, vol. 62, no. 23, pp. 15299–15302, Dec. 2000.
[43] M. Nagel, P. H. Bolivar, and H. Kurz, "Modular parallel-plate THz components for cost-efficient biosensing systems," *Semiconduct. Sci. Technol.*, vol. 20, pp. S281–S285, Jun. 2005.
[44] C. Janke, M. Först, M. Nagel, H. Kurz, and A. Bartels, "Asynchronous optical sampling for high-speed characterization of integrated resonant terahertz sensors," *Opt. Lett.*, vol. 30, no. 11, pp. 1405–1407, Jun. 2005.
[45] R. Mendis and D. Grischkowsky, "Undistorted guided wave propagation of sub-picosecond THz pulses," *Opt. Lett.*, vol. 26, no. 11, pp. 846–848, Jun. 2001.
[46] R. Mendis and D. Grischkowsky, "Terahertz interconnect with low loss and low group velocity dispersion," *IEEE Microw. Wireless Compon. Lett.*, vol. 11, no. 11, pp. 444–446, Nov. 2001.
[47] S. Coleman and D. Grischkowsky, "A THz TEM-mode two dimensional interconnect layer incorporating quasi-optics," *Appl. Phys. Lett.*, vol. 83, no. 18, pp. 2841–2843, Nov. 2003.
[48] J. Dai, S. Coleman, and D. Grischkowsky, "Planar THz quasi-optics," *Appl. Phys. Lett.*, vol. 85, no. 6, pp. 884–886, Aug. 2004.
[49] J. B. Pendry and A. MacKinnon, "Calculation of photon dispersion relations," *Phys. Rev. Lett.*, vol. 69, no. 19, pp. 2772–2775, Nov. 1992.
[50] J. B. Pendry, "Calculating photonic band structure," *J. Phys., Condens. Matter*, vol. 8, pp. 1085–1108, Feb. 1996.
[51] A. L. Reynolds, Translight Software, Based on the Transfer Matrix Method (TMM). ver. Pre-Beta, Univ. Glasgow, Glasgow, U.K., Sep. 2000.
[52] H. Lorenz, M. Despont, N. Fahrni, N. LaBianca, P. Renaud, and P. Vettiger, "SU-8: A low-cost negative resist for MEMS," *J. Micromech. Microeng.*, vol. 7, pp. 121–124, Apr. 1997.
[53] M. van Exter and D. Grischkowsky, "Characterization of an optoelectronic terahertz beam system," *IEEE Trans. Microw. Theory Tech.*, vol. 38, no. 11, pp. 1684–1691, Nov. 1990.
[54] A. J. Gatesman, J. Waldman, M. Ji, C. Musante, and S. Yngvesson, "An anti-reflection coating for silicon optics at terahertz frequencies," *IEEE Microw. Guided Wave Lett.*, vol. 10, no. 7, pp. 264–266, Jul. 2000.
[55] J. W. Digby, C. E. McIntosh, G. M. Parkhurst, B. M. Towlson, S. Hadjiloucas, J. W. Bowen, J. M. Chamberlain, R. D. Pollard, R. E. Miles, D. P. Steenson, L. S. Karatzas, N. J. Cronin, and S. R. Davies, "Fabrication and characterization of micromachined rectangular waveguide components for use at millimeter wave and terahertz frequencies," *IEEE Trans. Microw. Theory Tech.*, vol. 48, no. 8, pp. 1293–1303, Aug. 2000.
[56] S. Hadjiloucas, R. K. H. Galvao, J. W. Bowen, R. Martini, M. Brucherseifer, H. P. M. Pellemans, P. H. Bolivar, H. Kurz, J. Digby, G. M. Parkhurst, and J. M. Chamberlain, "Measurement of propagation constant in waveguide with wideband coherent terahertz spectroscopy," *J. Opt. Soc. Amer. B, Opt. Phys.*, vol. 20, no. 2, pp. 391–401, Feb. 2003.
[57] M. Van Exter and D. Grischkowsky, "Carrier dynamics of electrons and holes in moderately doped silicon," *Phys Rev. B, Condens. Matter*, vol. 41, no. 17, pp. 12140–12149, Jun. 1990.
[58] M. Born and E. Wolf, *Principles of Optics*. Cambridge, U.K.: Cambridge Univ. Press, 1999.
[59] P. A. Rizzi, *Microwave Engineering: Passive Circuits*. Englewood Cliffs, NJ: Prentice-Hall, 1988.
[60] S. Ramo, J. R. Whinnery, and T. Van Duzer, *Fields and Waves in Communication Electronics*. New York: Wiley, 1994.
[61] M. A. Ordal, L. L. Long, R. J. Bell, S. E. Bell, R. W. Alexander, Jr., and C. A. Ward, "Optical properties of the metals Al, Co, Cu, Au, Fe, Pb, Mo, Ni, Pd, Pt, Ag, Ti, and W in the infrared and far infrared," *Appl. Opt.*, vol. 22, no. 7, pp. 1099–1119, Apr. 1983.
[62] M. Qiu and S. He, "Numerical method for computing defect modes in two-dimensional photonic crystals with dielectric or metallic inclusions," *Phys. Rev. B, Condens. Matter*, vol. 61, no. 19, pp. 12871–12876, May 2000.

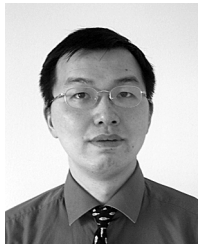

Yuguang Zhao (M'06) received the B.S. degree from Northwest Polytechnic University, Shaanxi Province, China, in 1993, the M.S. degree from Rensselaer Polytechnic Institute, Troy, NY, in 2002, and the Ph.D. degree from Oklahoma State University, Stillwater, in 2006.

His current research interests are terahertz devices, ultrafast opto-electronics, generation and applications of terahertz radiation, and ultrashort electrical pulse propagation in photonic crystals, and broadband terahertz waveguides.

Daniel R. Grischkowsky (SM'90–F'92) received the B.S. degree from Oregon State University, Corvallis, in 1962, and the Ph.D. degree from Columbia University, New York, NY, in 1968.

In 1969, he joined the IBM T. J. Watson Research Center, Yorktown Heights, NY. In 1993, he joined Oklahoma State University, Stillwater, where his research has concentrated on unique applications of THz-TDS, including waveguides, the Sommerfeld wave, surface waves, hole arrays, and photonic crystals.

Dr. Grischkowsky is a Fellow of the Optical Society of America (OSA) and the American Physical Society. He was the recipient of the 1985 Boris Pregel Award presented by the New York Academy of Sciences, the OSA 1989 R. W. Wood Prize, and the OSA 2003 William F. Meggers Award.